Resonant tunneling of surface plasmon polariton in the plasmonic nano-cavity

Junghyun Park[1], Hwi Kim[1], Il-Min Lee[1], Seyoon Kim[1], Jaehoon Jung[2], and Byoungho Lee[1*]

[1]National Creative Research Center for Active Plasmonics Application Systems
Inter-University Semiconductor Research Center and School of Electrical Engineering
Seoul National University, Gwanak-Gu Sillim-Dong, Seoul, 151-744, Korea
[2]Department of Electronics and Electrical Engineering, Dankook University
Yongin-Si, Gyeonggi-Do, 140-714, Korea
**Corresponding author: byoungho@snu.ac.kr*
http://oeqelab.snu.ac.kr

Abstract: We investigate the reflection and transmission characteristics of the low-dielectric constant cut off barrier in the metal-insulator-metal (MIM) waveguide and propose a novel plasmonic nano-cavity made of two cut off barriers and the waveguide between them. It is shown that the anti-symmetric mode in the MIM waveguide with the core of the low dielectric constant below the specific value cannot be supported and this region can be regarded as a cut off barrier with high stability. The phase shift due to the reflection at the finite-length cut off barrier is calculated and the design scheme of the cavity length for the resonant tunneling is presented. The transmission spectra through the proposed nano-cavity are also discussed.

OCIS codes: (240.6680) Surafce plasmons; (230.7390) Waveguides, planar; (140.3948) Microcavity devices.

References and links

1. H. Rather, *Surface Plasmons* (Springer-Verlag, Berlin, 1988).
2. W. L. Barnes, A. Dereux, and T. W. Ebbesen, “Surface plasmon subwavelength optics,” Nature **424**, 824-830 (2003).
3. S. Kim, H. Kim, Y. Lim, and B. Lee, “Off-axis directional beaming of optical field diffracted by a single subwavelength metal slit with asymmetric dielectric surface gratings,” Appl. Phys. Lett. **90**, 051113 (2007).
4. H. Kim, J. Hahn, and B. Lee, “Focusing properties of surface plasmon polariton floating dielectric lenses,” Opt. Express **16**, 3049-3057 (2008).
5. Y. Lim, S. Kim, H. Kim, J. Jung, and B. Lee, “Interference of surface plasmon waves and plasmon coupled waveguide modes for the pattering of thin film,” IEEE J. Quant. Electron. **44**, 305-311 (2008).
6. I.-M. Lee, J. Jung, J. Park, H. Kim, and B. Lee, “Dispersion characteristics of channel plasmon polariton waveguides with step-trench-type grooves,” Opt. Express **15**, 16596-16603 (2007).
7. S. Sidorenko and O. J. F. Martin, “Resonant tunneling of surface plasmon-polaritons,” Opt. Express **15**, 6380-6388 (2007).
8. M. I. Stockman, “Slow propagation, anomalous absorption, and total external reflection of surface plasmon polaritons in nanolayer systems,” Nano Lett. **6**, 2604-2608 (2006).
9. S. I. Bozhevolnyi and T. Søndergaard, “General properties of slow-plasmon resonant nanostructures: nano-antennas and resonators,” Opt. Express **15**, 10869-10877 (2007).
10. G. D. Valle, T. Søndergaard, and S. I. Bozhevolnyi, “Plasmon-polariton nano-strip resonators: from visible to infra-red,” Opt. Express **16**, 6867-6876 (2008).
11. H. T. Miyazaki and Y. Kurokawa, “Squeezing visible light waves into a 3-nm-thick and 55-nm-long plasmon cavity,” Phys. Rev. Lett. **96**, 097401 (2006).
12. Y. Kurokawa and H. T. Miyazaki, “Metal-insulator-metal plasmon nanocavities: analysis of optical properties,” Phys. Rev. B **75**, 035411 (2007).
13. H. T. Miyazaki and Y. Kurokawa, “Controlled plasmon resonance in closed metal/insulator/metal nanocavities,” Appl. Phys. Lett. **89**, 211126 (2006).
14. J. A. Dionne, L. A. Sweatlock, and H. A. Atwater, “Plasmon slot waveguides: Towards chip-scale propagation with subwavelength-scale localization,” Phys. Rev. B **73**, 035407 (2006).

#100290 - $15.00 USD Received 18 Aug 2008; revised 3 Oct 2008; accepted 4 Oct 2008; published 8 Oct 2008

15. R. Zia, M. D. Selker, P. B. Catrysse, and M. Brongersma, "Geometries and materials for subwavelength surface plasmon modes," J. Opt. Soc. Am. A **21**, 2442-2446 (2004).
16. E. N. Economou, "Surface plasmons in thin films," Phys. Rev. **182**, 539-554 (1969).
17. J. J. Burke, G. I. Stegeman, and T. Tamir, "Surface-polariton-like waves guided by thin, lossy metal films," Phys. Rev. B **33**, 5186-5201 (1986).
18. P. Berini, "Plasmon-polariton waves guided by thin lossy metal films of finite width: bound modes of symmetric structures," Phys. Rev. B **61**, 10484-10503 (2000).
19. J. A. Dionne, L. A. Sweatlock, and H. A. Atwater, "Planar metal plasmon waveguides: Frequency-dependent dispersion, propagation, localization, and loss beyond the free electron model," Phys. Rev. B **72**, 075405 (2005).
20. J. Park and B. Lee, "An approximate formula of the effective refractive index of the metal-insulator-metal surface plasmon polariton waveguide in the infrared region," Jpn. J. Appl. Phys. (accepted for publication).
21. J. A. Dionne, H. J. Lezec, and H. A. Atwater, "Highly confined photon transport in subwavelength metallic slot waveguides," Nano Lett. **6**, 1928-1932 (2006).
22. M. J. Preiner, K. T. Shimizu, J. S. White, and N. A. Melosh, "Efficient optical coupling into metal-insulator-metal plasmon mode with subwavelength diffraction gratings," Appl. Phys. Lett. **92**, 113109 (2008).
23. B. Wang and G. P. Wang, "Plasmon Bragg reflectors and nanocavities on flat metallic surfaces," Appl. Phys. Lett. **87**, 013107 (2005).
24. A. Hosseini and Y. Massoud, "A low-loss metal-insulator-metal plasmonic Bragg reflector," Opt. Express **14**, 11318-11323 (2006).
25. Z. Han, E. Forsberg, and S. He, "Surface plasmon Bragg gratings formed in metal-insulator-metal waveguides," IEEE Photon. Technol. Lett. **19**, 91-93 (2007).
26. J. Park, H. Kim, and B. Lee, "High order plasmonic Bragg reflection in the metal-insulator-metal waveguide Bragg grating," Opt. Express **16**, 413-425 (2008).
27. B. E. A. Saleh and M. C. Teich, *Fundamentals of Photonics*, 2nd ed. (Wiley Intersceince, Hoboken, NJ, 2007).
28. H. J. Lezec, J. A. Dionne, and H. A. Atwater, "Negative refraction at visible frequencies," Science **316**, 430-432 (2007).
29. M. G. Moharam and T. K. Gaylord, "Rigorous coupled-wave analysis of planar-grating diffraction," J. Opt. Soc. Am. A **71**, 811-818 (1981).
30. M. G. Moharam, E. B. Grann, and D. A. Pommet, "Formulation for stable and efficient implementation of the rigorous coupled-wave analysis of binary gratings," J. Opt. Soc. Am. A **12**, 1067-1076 (1995).
31. P. Lalanne, "Improved formulation of the coupled-wave method for two-dimensional gratings," J. Opt. Soc. Am. A **14**, 1592-1598 (1997).
32. H. Kim, I.-M. Lee, and B. Lee, "Extended scattering-matrix method for efficient full parallel implementation of rigorous coupled-wave analysis," J. Opt. Soc. Am. A **24**, 2313-2327 (2007).
33. K.-Y. Kim, "Photon tunneling in composite layers of negative- and positive-index media," Phys. Rev. E **70**, 047603 (2004)
34. K.-Y. Kim and B. Lee, "Complete tunneling of light through impedance-mismatched barrier layers," Phys. Rev. A **77**, 023822 (2008).
35. J. Park, K.-Y. Kim, and B. Lee, "Complete tunneling of light through a composite barrier consisting of multiple layers," (in submission).

---

1. Introduction

In conventional dielectric waveguide it is impossible to confine the light in subwavelength scale due to the diffraction limit. Recently there have been various theoretical and experimental studies to overcome this fundamental limit and surface plasmon polaritons (SPPs) are believed to be one of the most promising methods [1, 2]. SPPs are quasi-particles arising from the coupling between electromagnetic waves and oscillations of conduction electrons at interface between a metal and a dielectric. Extensive studies for fundamental properties and applications have been carried out [3-6]. Resonant tunneling phenomena of the SPP mode have been widely studied [7-13]. As a fundamental device, lots of researches on the SPP-based waveguide have been carried out [14-20]. Among them, the metal-insulator-metal (MIM) waveguide has been known to be able to support the propagating mode within the subwavelength modal size with the considerable propagation length [14, 15]. In addition to basic studies on the propagating property of various kinds of the MIM-type waveguides, there have been diverse researches for the practical use of them, such as the fabrication [21] and the coupling method [22], and the wavelength-selective transmission property [23-26].

The wavelength-selective device can be a building block of the de-multiplexer which is used to separate each signal channel with different wavelength. There have been suggested lots of wavelength-selective devices [23-25]. Those employ the Fabry-Perot effect and mainly consist of two parts: two mirrors and the waveguide between them. To make a mirror-like structure, we can think of the waveguide Bragg grating (WBG) structures composed of alternatively stacked regions with different types of the core, the cladding, or the core width. And by introducing an artificial defect in the periodicity one can implement a wavelength-selective device. It was reported that we can also make use of the higher order of Bragg reflections as well [26].

However, those WBG-based wavelength-selective devices require several numbers of gratings, resulting in the unavoidable long structure. In this paper, we study the cut off property of the MIM waveguide and suggest a resonant tunneling of the SPP mode through the plasmonic nano-cavity composed of two cut off barriers and the MIM waveguide between them. The key idea we come up with is that the WBG region for the mirror-like function can be replaced by the cut off *barrier* made of a transparent dielectric core with the low dielectric constant, not an intrinsically opaque metal. In the conventional dielectric waveguide, cut off of a mode means that the power confinement in the cladding becomes larger than that in the core and there can still be power transmission through the cladding [27]. Unlikely, cut off in the MIM waveguide prevents the power from propagating not only through the core but also through the cladding due to the opaque metal cladding. It will be shown that the proposed structure can be used to make the wavelength-selective device with the considerably short length.

This paper is organized as follows. Firstly, we examine the propagating property of the MIM waveguide focusing on the cut off property. Then, the reflection and transmission properties of the cut off barrier with the finite length are investigated. Next we examine the transmission characteristics through the Fabry-Perot structure consisting of two barriers and the waveguide between them. The discussion of the cavity properties such as quality (Q) factor is also presented.

2. Cut off properties of the MIM waveguide

In this section, we characterize the cut off properties of the MIM waveguide. Starting from the analysis of the propagating mode in the MIM waveguide, we will discuss the cut off condition of the MIM waveguide. It will be shown that there is a specific regime of material and geometrical parameters, in which no propagation mode exists.

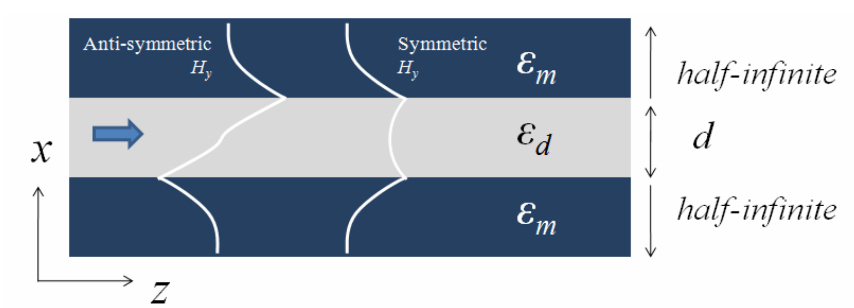

Fig. 1. Metal-insulator-metal surface plasmon polariton waveguide.

Let us consider the propagating mode of the MIM waveguide (Fig. 1). The core is a dielectric material with dielectric function ε_d and width d. The cladding is a metal and its dielectric function, ε_m, is described by the Drude model as follows:

#100290 - $15.00 USD Received 18 Aug 2008; revised 3 Oct 2008; accepted 4 Oct 2008; published 8 Oct 2008

$$\varepsilon_m = \varepsilon_\infty - \frac{\omega_p^2}{\omega(\omega + i\gamma)}, \tag{1}$$

where ε_∞ is the infinite frequency dielectric constant, ω_p the bulk plasma frequency, ω the angular frequency, and γ the collision frequency which is related to the dissipation loss in the metal. We assume that the metal is silver ($\varepsilon_\infty = 3.7$, $\omega_p = 9\text{eV}$, and $\gamma = 0.018\text{eV}$) [26]. Note that we express ω_p, ω, and γ in a form of the photon energy by multiplying the Planck's constant $\hbar$ [26]. It is known that ε_m is negative in the optical frequency regime, where ω has range from ~2eV to ~4eV. And its absolute value decreases with increasing ω, and ε_m can even be positive. We assume the monochromatic operation with the free space wavenumber $k_0 = \omega / c_0$, the time-dependency of $\exp(-j\omega t)$, and corresponding free space wavenumber $\lambda_0 = 2\pi / k_0$. Here, c_0 is the speed of the light in vacuum. We consider the TM mode (p-polarized), so that H_x, E_y, and H_z are all zero. Since the propagating properties of the three-dimensional MIM waveguide do not vary so much from those of the two-dimensional structure even if the vertical height is reduced to subwavelength, we think our analysis can elucidate the properties of the MIM waveguide without much loss of generality [21].

The propagating modes that can be supported in the MIM waveguide are classified into 4 types according to their field distribution: the photonic anti-symmetric mode, the photonic symmetric mode, the plasmonic anti-symmetric mode, and the plasmonic symmetric mode. The photonic modes mean that the field distributions in the core are sinusoidal, whereas the plasmonic modes correspond to the exponentially decaying fields. The anti-symmetric and the symmetric modes are the guided modes with the anti-symmetric and the symmetric transverse electric and magnetic field distributions, respectively. The corresponding characteristic equations are given as follows [20]:

$$\text{photonic symmetric mode} : \tan\left(\frac{k_d d}{2}\right) = \frac{\varepsilon_d \kappa_m}{\varepsilon_m k_d}, \tag{2.a}$$

$$\text{photonic anti-symmetric mode} : \cot\left(\frac{k_d d}{2}\right) = -\frac{\varepsilon_d \kappa_m}{\varepsilon_m k_d}, \tag{2.b}$$

$$\text{plasmonic symmetric mode} : \tanh\left(\frac{\kappa_d d}{2}\right) = -\frac{\varepsilon_d \kappa_m}{\varepsilon_m \kappa_d}, \tag{2.c}$$

$$\text{plasmonic anti-symmetric mode} : \coth\left(\frac{\kappa_d d}{2}\right) = -\frac{\varepsilon_d \kappa_m}{\varepsilon_m \kappa_d}. \tag{2.d}$$

Here, k_d, κ_d, and κ_m denote the transverse wavenumber in the core of the photonic mode, that in the core of the plasmonic mode, and that in the cladding, respectively. Note that the sign of the right hand side in Eq. (2.a) is positve, whereas those in Eqs. (2.b) to (2.d) are negative. The origin of the difference can be found in Refs. 14 and 19. The momentum conservation condition yields

$$k_d^2 + \beta^2 = \varepsilon_d k_0^2, \tag{3.a}$$

$$-\kappa_d^2 + \beta^2 = \varepsilon_d k_0^2, \tag{3.b}$$

$$-\kappa_m^2 + \beta^2 = \varepsilon_m k_0^2, \tag{3.c}$$

#100290 - $15.00 USD Received 18 Aug 2008; revised 3 Oct 2008; accepted 4 Oct 2008; published 8 Oct 2008

where β is the longitudinal wavenumber. Note that β is common both in the dielectric core and the metal cladding due to the phase matching conditon. Combining Eqs. (2.a)-(2.d) and Eqs. (3.a)-(3.c), we can obtain β. When the dielectric constants possess imaginary term, β should be complex. The effective refractive index of the propagating mode is defined as $n_{eff} = \mathrm{Re}(\beta / k_0)$. Whether the propagating mode is the photonic mode or the plasmonic mode depends on the relation between n_{eff} and $\sqrt{\varepsilon_d}$, i.e., the mode is called the photonic mode if $n_{eff} \le \sqrt{\varepsilon_d}$ whereas it is called the plasmonic mode if $n_{eff} \ge \sqrt{\varepsilon_d}$. In addition, it is known that the fundamental anti-symmetric mode can be either the photonic or plasmonic modes [14]. This property will be discussed later. The propagation length at which the field intensity decreases by $1/e$ is given by $L_p = \left(2\,\mathrm{Im}(\beta)\right)^{-1}$. It is of importance to understand the functional behavior of n_{eff} and L_p over material and geometrical parameters such as ε_d, d, and λ_0, and there have been lots of researches on their characteristics [14, 15]. Especially, for a specific condition there is no propagating mode in the MIM waveguide, which is called cut off. In this paper, we focus on the cut off property of the propagating mode.

In Figs. 2(a)-(d), we illustrate n_{eff} (solid line) and L_p (dotted line) as a function of ε_d and d. Figures 2(a) and (c) correspond to the symmetric mode and Figs. 2(b) and (d) the anti-symmetric mode. In Fig. 2(a), we observe that as ε_d increases, n_{eff} of the symmetric mode increases and L_p decreases. When ε_d becomes close to $|\varepsilon_m|$ described by the vertical dashed line, n_{eff} grows dramatrically and L_p goes to zero. For $\varepsilon_d > |\varepsilon_m|$, there is no symmetric mode, i.e., cut off. This can be ascribed to the fact that each interface between the core and the upper (lower) cladding cannot support a SPP mode for $\varepsilon_d > |\varepsilon_m|$. In other words, the wavenumber of the single interface SPP mode [1],

$$k_{S.I.SPP} = k_0 \sqrt{\frac{\varepsilon_m \varepsilon_d}{\varepsilon_m + \varepsilon_d}}\,, \tag{4}$$

is complex-valued for $\varepsilon_d > |\varepsilon_m|$. It is also seen that cut off does not occur in the low ε_d regime. Figure 2(b) illustrates n_{eff} and L_p of the anti-symmetric mode. Likewise to the symmetric case, n_{eff} increases and L_p decreases with increasing ε_d. When ε_d approaches $|\varepsilon_m|$ (the right vertical dashed line), n_{eff} diverges and L_p becomes zero, i.e., cut off. The origin of this kind of cut off is the same as that in the symmetric case: there is no single interface SPP mode for $\varepsilon_d > |\varepsilon_m|$. It should be mentioned that when the core width is extremely small, there can be the anti-symmetric mode with the considerable propagating length. In this case, the signs of the real and imaginary parts of β are opposite, which means that the power flows in the opposite direction to the phase, i.e., negative effective refractive index. There has been reported an experimental demonstration for this kind of negative refraction effects by Lezec *et al*. [28].

Let us now consider the low-ε_d regime. Behaviours of n_{eff} and L_p of the anti-symmetric mode are different from those of the symmetric mode. In the anti-symmetric mode they become zero as ε_d decreases to a critical point, i.e. another type of cut off. Considering that n_{eff} becomes zero at this critical point, we can derive this point from an implicit function. Note that the anti-symmetric mode should not be the plasmonic mode but the photonic mode near the low-ε_d cut off point. This is because this kind of cut off occurs as n_{eff} becomes zero, which means n_{eff} should be smaller than $\sqrt{\varepsilon_d}$. Hence we invoke Eqs. (2.b), (3.a), and (3.c) to calculate the low-ε_d cut off condition. Substitution of $\beta = 0$ into Eqs. (3.a) and (3.c) and combining them with Eq. (2.b) result in the following condition:

$$\cot\left(\frac{k_0 d}{2}\sqrt{\varepsilon_{cut\,off}}\right) - \sqrt{\frac{\varepsilon_{cut\,off}}{-\varepsilon_m}} = 0 . \tag{5}$$

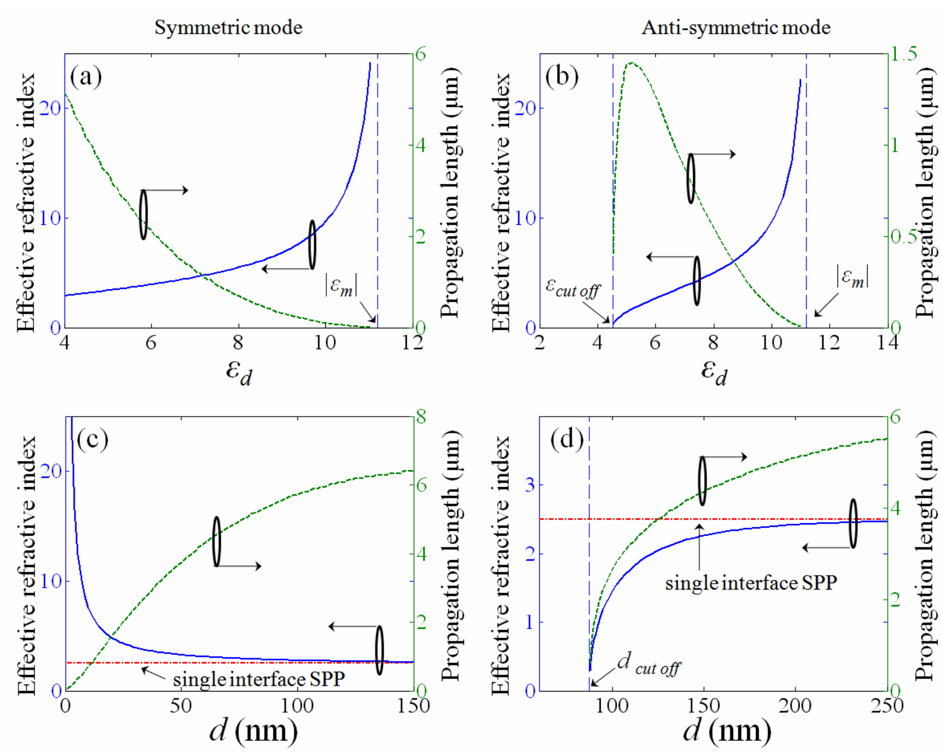

Fig. 2. Effective refractive index and the propagation length as a function of (a) ε_d in the symmetric mode, (b) ε_d in the anti-symmetric mode, (c) d in the symmetric mode, and (d) d in the anti-symmetric mode. $d = 80\text{nm}$ in (a) and (b). $\varepsilon_d = 4$ in (c) and (d). $\lambda_0 = 532\text{nm}$ in all cases.

It should be mentioned that there is no exact real-valued ε_d ($\varepsilon_{cut\,off}$) satisfying Eq. (5) since only ε_m is complex. However, the imaginary part of ε_m is quite small compared to the real part. Thus the error from taking $|\varepsilon_m|$ instead of $-\varepsilon_m$ is negligible. For given parameters in Fig. 2(b), $\varepsilon_{cut\,off}$ satisfying Eq. (5) with $|\varepsilon_m|$ is obtained as 4.522, which is in good agreement with the cut off point observed in Fig. 2(b). The physical origin of this kind of cut off can be understood from the repulsive Coulomb force. Recalling that the anti-symmetric mode has the symmetic distribution of the collective oscillation of free electrons near the surface, i.e., the surface plasmons, we know that there is a repulsive force between the SPPs at upper and lower metal claddings, which pushes the SPPs into the metal cladding and prevents the SPP mode from propagating through the waveguide. Since the amplitude of this

#100290 - $15.00 USD Received 18 Aug 2008; revised 3 Oct 2008; accepted 4 Oct 2008; published 8 Oct 2008

repulsive force increases with decrease of ε_d, the mode is cut off below a critical value of $\varepsilon_{cut\,off}$. The reason why the propagation length of the anti-symmetric mode is usually shorter than that of the symmetric mode can be understood from this point of view as well.

Let us examine the cut off property arising from the narrow core. Figure 2(c) shows n_{eff} and L_p as a function of the core width for the symmetric mode. When the core is infinitely wide, the interference between the single interface SPP modes becomes weak and n_{eff} approaches $\mathrm{Re}\left(k_{S.I.SPP}/k_0\right)$. As the core width decreases, n_{eff} increases and L_p decreases, and cut off occurs when $d=0$. As a matter of fact, it is somewhat delicate to call this cut off. In other words, $d=0$ stands for the absence of the core, which means that there is no guiding structure. Contrary to the symmetric mode, however, n_{eff} of the anti-symmetric mode decreases with decreasing d and the anti-symmetric mode has a critical point of the core width below which no propagation mode exists (Fig. 2(d)). We can estimate the critical core width by using the fact that $n_{eff}=0$ at the point. Using Eq. (5), we express the cut off thickness as follows:

$$d_{cut\,off} = \frac{2}{k_0\sqrt{\varepsilon_d}}\cot^{-1}\sqrt{\frac{\varepsilon_d}{-\varepsilon_m}}\,. \tag{6}$$

For given parameters in Fig. 2(d), the cut off thickness with $|\varepsilon_m|$ instead of $-\varepsilon_m$ is calculated as 87nm, which coincides well with results (vertical dashed line in Fig. 2(d)). Table 1 summarizes the aforementioned cut off properties such as cut off ε_d and d for the symmetric and the anti-symmetric modes.

Table 1. Cut off conditions of ε_d and d.

	Symmetric mode	Anti-symmetric mode
ε_d	$\varepsilon_d > \|\varepsilon_m\|$	$\varepsilon_d > \|\varepsilon_m\|$ or $\varepsilon_d < \varepsilon_{cut\,off}$
d	$d \to 0$	$d < d_{cut\,off} = \frac{2}{k_0\sqrt{\varepsilon_d}}\cot^{-1}\left(\sqrt{\frac{\varepsilon_d}{-\varepsilon_m}}\right)$

Before closing this section, let us compare the concept of mode cut off in conventional dielectric slab waveguides and the MIM plasmonic waveguide. In conventional dielectric waveguides, the cut off is a state in which no guided modes can be supported through the core of the waveguide. It happens when the operating wavelength is much longer than the core width or the index difference between the core and the cladding is very small. It can be explained by using n_{eff}, which usually ranges from the refractive index of the cladding to that of the core. As the wavelength increases, or as the core width decreases, or, as the refractive index difference between the core and the cladding decreases, n_{eff} decreases and becomes close to the refractive index of the cladding. At a specific point where it becomes smaller than the cladding index, we say that the mode is cut off. However, it should be pointed out that, the light wave can radiate through the cladding even in the cut off state. This is because both the core and the cladding are transparent, which means that they can support the radiation of the plane wave. On the other hand, the metal cladding of the MIM waveguide is opaque itself. As can be seen in Eq. (3.c), the negative ε_m requires that the electromagnetic field in the cladding exponentially decay. Therefore no light energy can leak into the cladding at any

#100290 - $15.00 USD Received 18 Aug 2008; revised 3 Oct 2008; accepted 4 Oct 2008; published 8 Oct 2008

situation. When the mode is cut off, since neither the light energy be able to propagate through the core nor to leak into the cladding, it should be totally reflected. This is the fundamental difference between the cut off in conventional dielectric waveguides and the MIM plasmonic waveguide.

3. Reflection and transmission properties through *barrier* with finite length

In this section, based on the aforementioned cut off properties we examine the reflection and transmission properties through the finite-length MIM waveguide without a propagating mode. The cut off MIM waveguide region can be regarded as a *barrier*, since the incident wave is reflected by it. It will be shown that due to the finite length some of energy can be transmitted. The phase shift originating from the reflection will also be discussed.

Let us consider a MIM waveguide structure which is a cascade structure of three layers: a propagating region, a cut off region, and a propagating region (Fig. 3). There can be various combinations of material and geometrical parameters to form the cut off region. For the symmetric mode, the MIM waveguide with the core of high ε_d ($>|\varepsilon_m|$) or zero-d will prohibit the propagation. In the anti-symmetric mode, $\varepsilon_d > |\varepsilon_m|$, $\varepsilon_d < \varepsilon_{d,cut\,off}$, or $d < d_{cut\,off}$ can be used to form a barrier. In this paper, we focus on cut off of the anti-symmetric mode with low ε_d ($< \varepsilon_{d,cut\,off}$). Other configurations will be reported in the next publication.

Figure 3(a) shows the schematic diagram of the finite-length barrier in the MIM waveguide. The TM-polarized anti-symmetric mode is incident from the left side. The MIM waveguide with the core of ε_h supports the guided mode, whereas that of ε_l cannot. The latter acts as a barrier and most energy of the incident wave will be reflected. It should be mentioned that, although there can be symmetric propagating mode in the MIM waveguide with the core of ε_l, the incident anti-symmetric mode cannot be coupled into the symmetric mode owing to the geometrical symmetry. Meanwhile, since the length of barrier is finite, there can be transmitted energy by tunneling. This is reminiscent of the tunneling of electron through the potential barrier in the quantum mechanics (Fig. 3(b)).

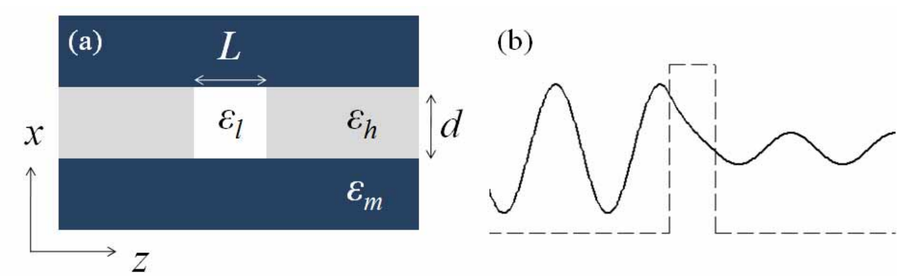

Fig. 3. (a) Finite-length barrier (ε_l) in the MIM waveguide with the core dielectric constant of ε_h. (b) Tunneling of electron through a potential barrier.

To examine the reflection and transmission properties, we used the rigorous coupled-wave analysis (RCWA) [29-32]. The main benefit from the RCWA is that we can distinguish energy of a mode from another.

In Fig. 4(a), we depict the reflection coefficient, $R = |r|^2$, and the phase shift due to the reflection, $\phi_{ref} = \arg(r)$, as a function of the barrier length, L, for various values of the permittivity of the cut off barrier ($\varepsilon_l = 2, 4, 4.3$). Here r denotes the reflection amplitude obtained by the RCWA. ε_h is chosen to be 6. d is set to be 80nm. The reflection coefficient scales with the barrier length. If ε_l is smaller than $\varepsilon_{cut\,off}$ obtained by Eq. (5), cut off occurs

#100290 - $15.00 USD Received 18 Aug 2008; revised 3 Oct 2008; accepted 4 Oct 2008; published 8 Oct 2008

(see Fig. 2(b)). As ε_l decreases, the barrier strength is enhanced, i.e., the reflection coefficient increases. With regard to the reflection phase shift, it is observed that as the barrier length decreases the reflection phase shift asymptotes to 90°. This is in good agreement with the result of the photon tunneling through a one-dimensional composite barrier [33-35]. As the barrier length increases, the reflection phase shifts for various values of ε_l 's also change and they asymptote to the specific values of their own. It is noteworthy that the reflection phase shift of the cut off barrier with $\varepsilon_l = 4$ remains almost constant around 90° since the asymptote value is also 90°. As will be discussed later, the reflection phase shift is necessary to calculate the cavity length. In other words, the resonant tunneling condition comes from the constructive interference between the propagating modes with the multiple reflections. When the overall phase shift that the propagating mode experiences during the single round trip becomes an integer multiple of 2π, the resonant tunneling occurs.

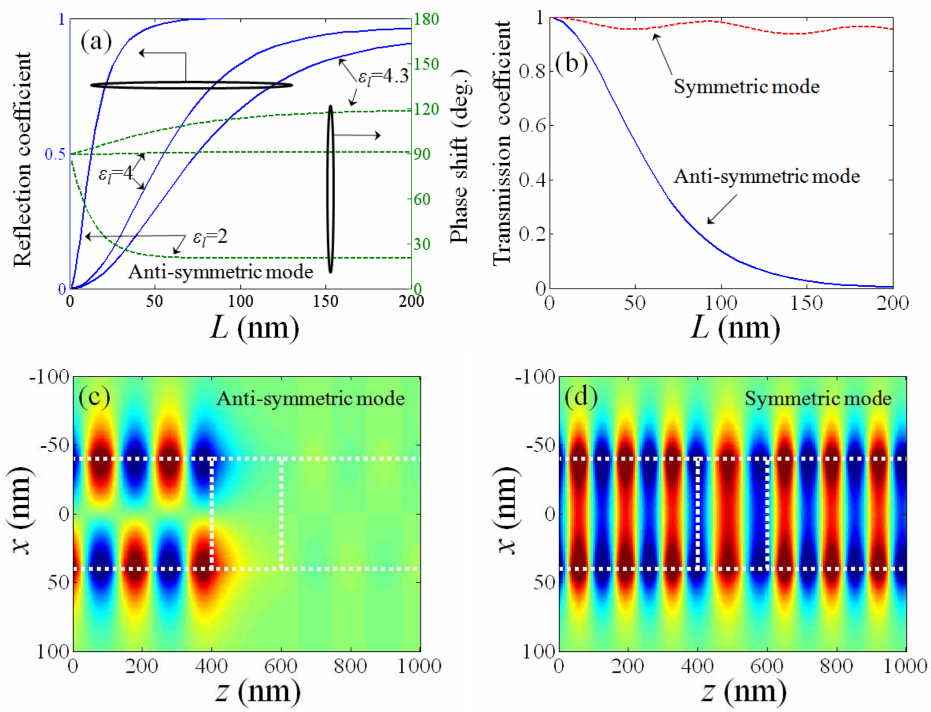

Fig. 4. (a) Reflection coefficient and phase shift due to the reflection as a function of the barrier length for the anti-symmetric mode. (b) Dependence of the transmission coefficient on the barrier length of the anti-symmetric and symmetric modes. Field distributions of H_y for (c) the anti-symmetric mode and (d) the symmetric mode with the barrier length of 200nm. $\varepsilon_h = 6$, $d = 80\text{nm}$, and $\lambda_0 = 532\text{nm}$ in all cases. $\varepsilon_l = 2, 4, 4.3$ in (a). $\varepsilon_l = 4$ in (b)-(d). The white dotted-lines show the boundaries of the structure shown in Fig. 3(a).

Figure 4(b) depicts the transmission coefficients, $T = |t|^2$, of the anti-symmetric (solid line) and the symmetric (dashed line) modes as a function of the barrier length, where t represents the transmission amplitude. Here the barrier is made of a low ε_d core, where the anti-symmetric mode is cut off. It is seen that the transmission coefficient decreases with increase of the barrier length and becomes less than 1% when the barrier length is 190nm. Contrary to the anti-symmetric mode, however, the symmetric mode can transmit through the low ε_d region. This is because the low ε_d region does not act as a barrier for the symmetric

#100290 - $15.00 USD Received 18 Aug 2008; revised 3 Oct 2008; accepted 4 Oct 2008; published 8 Oct 2008

mode. As we discussed above, the symmetric mode is not cut off with a low dielectric constant. Only the anti-symmetric mode feels the low ε_d as a barrier. The mode selective transmission property can be used for a mode filter.

We show in Fig. 4(c) the transverse magnetic (H_y) field distribution when the anti-symmetric mode is incident from the left side to the 200nm-length barrier. It is seen that most energy is reflected, giving rise to the standing wave at the incident region. Note that the period of the standing wave is about 20nm. This originates from the fact that n_{eff} of the anti-symmetric mode at the given structure parameters is 2.67 and thus the effective wavelength is 199.3nm. Please remind that the terminologies 'symmetric' and 'anti-symmetric' are based on H_y, thus the anti-symmetric mode distribution has a node line along the center line of the core. Figure 4(d) illustrates H_y field distribution for the symmetric mode. We can check that most energy of the symmetric mode can transmit through the low ε_d region.

One may be inclined to compare the strength of the cut off barrier and the WBG. By modulating the width of the dielectric constant of the core, one can make the MIM WBG through which guided modes with specific wavelengths cannot transmit. Figure 5(a) shows the schematic diagram of a MIM WBG with the core-index modulation. Two different kinds of core with dielectric constants of 6 and 5 are alternatively stacked with the period P of 130nm and the filling factor f of 0.5. N denotes the number of gratings. The period was chosen in such a way that the fundamental Bragg reflection occurs at the wavelength of 532nm. We investigated the transmission property through the MIM WBG as a function of the number of gratings (Fig. 5(b)). The more gratings we use, the less the transmission becomes. However, in order to achieve the transmission less than 1%, more than 9 gratings are needed, which leads to the total length of 1.1μm.

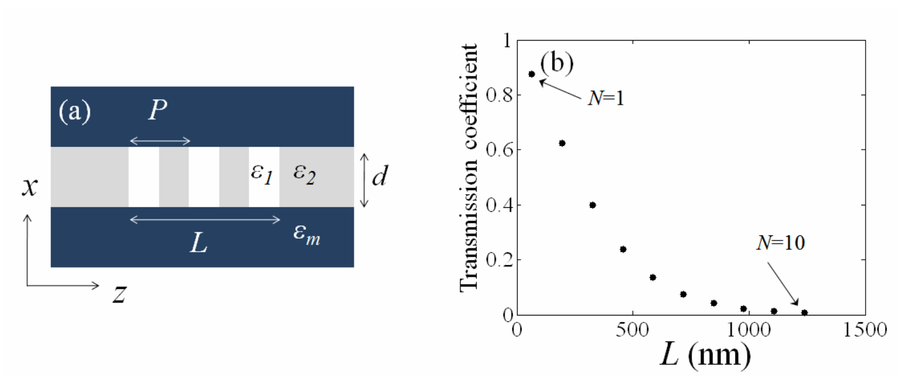

Fig. 5. (a) Schematic diagram of the MIM waveguide Bragg grating. (b) Transmission as a function of the grating number. $\varepsilon_2 = 6$, $\varepsilon_1 = 5$, $d = 80\text{nm}$, $P = 130\text{nm}$, $f = 0.5$, and $\lambda_0 = 532\text{nm}$.

4. Resonant tunneling of the SPPs through the plasmonic nano-cavity

We are now led to discussion on the transmission property through the plasmonic nano-cavity which is composed of two cascaded cut off barriers with the distance L_2 (see Fig. 6(a)). Owing to the finite length of the first cut off barrier, some of energy of the incident anti-symmetric mode can transmit by the tunneling and multiple reflections occur between two cut off barriers. If the overall phase shift that the propagating mode experiences, which is given by $\psi = 2\left(2\pi n_{eff} L_2 / \lambda_0 + \phi_{ref}\right)$, becomes an integer multiple of 2π, the constructive

#100290 - $15.00 USD Received 18 Aug 2008; revised 3 Oct 2008; accepted 4 Oct 2008; published 8 Oct 2008

interference results in the resonant tunneling. The cavity length for the q-th resonant tunneling is hence obtained as follows:

$$L_2 = \frac{\lambda_0}{2n_{eff}}\left(q - \frac{\phi_{ref}}{\pi}\right), \qquad (q = 1, 2, 3, \ldots). \tag{7}$$

In Fig. 6(b), we show the transmission coefficient of the anti-symmetric mode as a function of the cavity length (L_2) for various values of the barrier length (L_1). The arrow related with L_1 indicates the trend of decreasing L_1 from 80nm to 40nm. Several transmission peaks are observed. Note that n_{eff} is 2.676 and ϕ_{ref} is 90°. The first transmission peak at the L_2 of 50nm corresponds to the first resonant tunneling mode and we can see the second and third modes at 149nm and 249nm, respectively. It is noteworthy that the cavity length for the fundamental resonance is much smaller than the half wavelength, $\lambda_0/(2n_{eff})$.

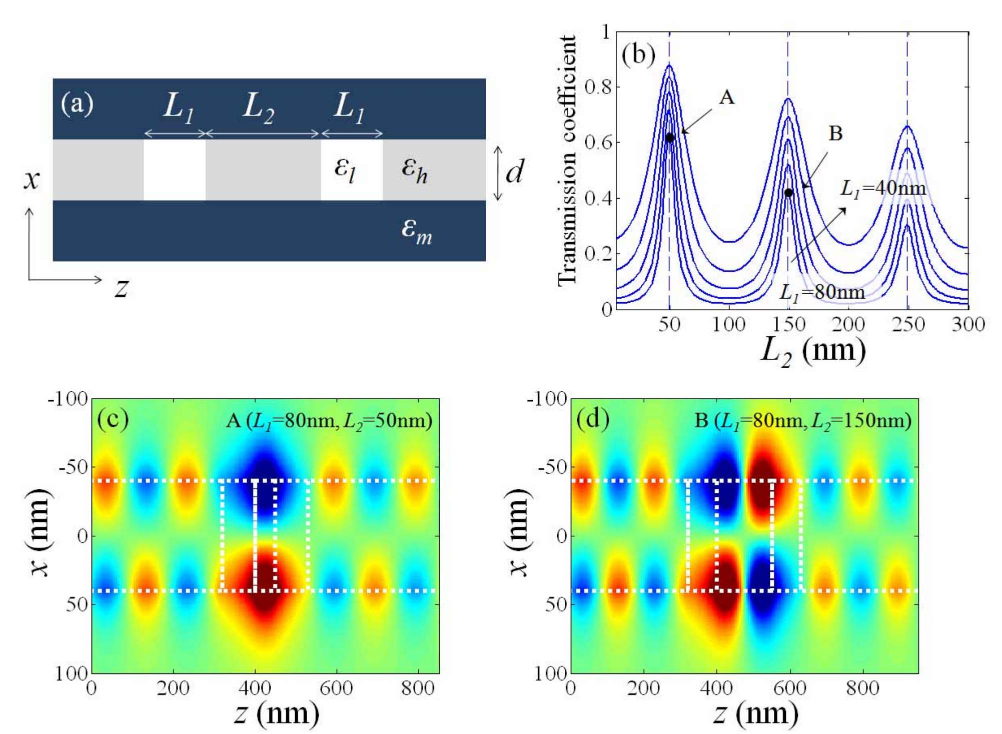

Fig. 6. (a) Schematic diagram of the MIM Fabry-Perot cavity consisting of two cut off barriers and the waveguide between them. (b) Dependence of the transmission coefficient on the length of the cavity for various values of barrier lengths. H_y field distributions at (c) the point A (the first resonance mode) and (d) the point B (the second resonance mode). $\varepsilon_h = 6$, $\varepsilon_l = 4$, $d = 80\text{nm}$, and $\lambda_0 = 532\text{nm}$ in all cases. The white dotted-lines show the boundaries of the structure shown in part (a).

The peak transmission coefficient value decreases with increase of the order of the resonance mode owing to the dissipation loss in the metal. As the cut off barrier length decreases from 80nm to 40nm, the transmission coefficients increase, whereas the L_2 values of transmission maxima remain unchanged. This is due to the fact that the reflection phase shift is nearly independent of the barrier length for $\varepsilon_l = 4$, as seen in Fig. 4(a). The dashed vertical lines (from left to right) in Fig. 6(b) indicate L_2 of 50nm, 149nm, and 249nm,

#100290 - $15.00 USD Received 18 Aug 2008; revised 3 Oct 2008; accepted 4 Oct 2008; published 8 Oct 2008

respectively. To verify the results, we show in Figs. 6(c) and (d) the transverse magnetic field distributions at the first (point A) and the second (point B) resonance modes. A node line along the center of the cavity in the transverse direction is observed for the second mode, whereas no node line is observed for the first resonance mode.

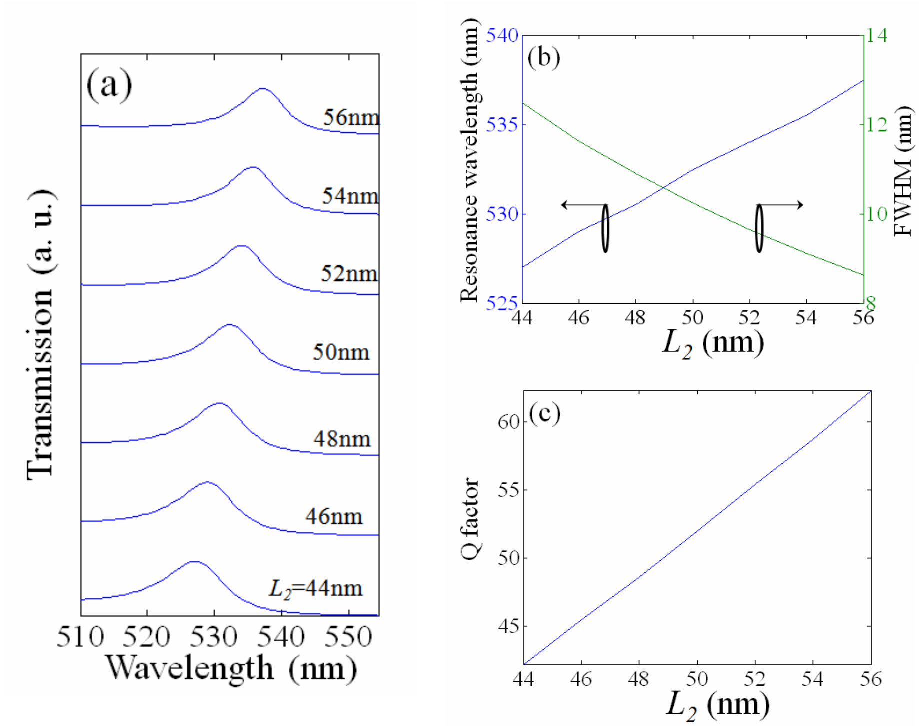

Fig. 7. (a) Transmission spectra for various values of the cavity lengths (L_2). (b) Resonance wavelength and the full-width at half maximum (FWHM) as a function of the cavity length. (c) Q factor versus the cavity length. $\varepsilon_h = 6$, $\varepsilon_l = 4$, $d = 80\text{nm}$, $L_1 = 80\text{nm}$ and $\lambda_0 = 532\text{nm}$ in all cases.

Based on the aforementioned cavity properties, we investigated the transmission coefficient as a function of the operating wavelength. Figure 7(a) illustrates the transmission spectra for various values of cavity lengths for the fundamental resonance mode. It is observed that the resonance wavelength increases as the cavity length gets longer. Therefore by arranging the plasmonic nano-cavities with different cavity lengths we can selectively transmit the channels with different carrier frequencies. In Fig. 7(b), we depict the resonance wavelength (left *y*-axis) and the full-width at half maximum (FWHM, right *y*-axis) as a function of the cavity length for the fundamental resonance mode. It is seen that the resonance wavelength scales with the cavity length, whereas the FWHM decreases with increase of the cavity length. The *Q* factor defined as the resonance wavelength normalized by the FWHM is shown in Fig. 7(c). We obtain *Q* factor of 52 at the resonance wavelength of 532nm. The *Q* factor can be improved by using a longer cut off barrier. The *Q* factor is related to the finesse factor, which is governed by the effective overall distributed-loss coefficient [27]. If the length of the cut off barrier increases, the reflectance of each single barrier also increases, resulting in the higher *Q* factor. On the other hand, the longer cut off barrier exhibits the higher absorption by the barrier, resulting in the degradation of the total transmission energy.

#100290 - $15.00 USD Received 18 Aug 2008; revised 3 Oct 2008; accepted 4 Oct 2008; published 8 Oct 2008

5. Conclusion

In this paper, we examined the reflection and transmission properties of the cut off barrier in the MIM waveguide and investigated the resonant tunneling of the SPP mode through the plasmonic nano-cavity consisting of two cut off barriers and the MIM waveguide between them. It turned out that the MIM waveguide with the core of the low dielectric constant below the specific value ($\varepsilon_{cut\,off}$) cannot support the anti-symmetric mode and can be used as a cut off barrier. The reflection from and transmission through a single cut off barrier was investigated. Based on the reflection and transmission properties, we can calculate the cavity length for a specific resonance wavelength, which is in good agreement with our simulation results. The *Q* factor of the proposed structure is about 52. We believe that the proposed structure can be used to implement a wavelength-selective device for the subwavelength-scale integrated nano-photonic circuits.

Acknowledgment

This work was supported by Ministry of Education, Science and Technology of Korea and Korea Science and Engineering Foundation through the Creative Research Initiatives Program (Active Plasmonics Application Systems).